The use of photothermal techniques for thermal conductivity and thermal boundary resistance measurements of phase-change chalcogenides alloys

ⓘD Jean-Luc Battaglia, Andrzej Kusiak and ⓘD Kanka Ghosh

COLLECTIONS

Paper published as part of the special topic on Photothermics

View Online   Export Citation   CrossMark

ARTICLES YOU MAY BE INTERESTED IN

Heterogeneously structured phase-change materials and memory
Journal of Applied Physics **129**, 050903 (2021); https://doi.org/10.1063/5.0031947

Probing thermal conductivity of subsurface, amorphous layers in irradiated diamond
Journal of Applied Physics **129**, 055307 (2021); https://doi.org/10.1063/5.0038972

Crystallization properties of melt-quenched Ge-rich GeSbTe thin films for phase change
memory applications
Journal of Applied Physics **128**, 155105 (2020); https://doi.org/10.1063/5.0023696

The use of photothermal techniques for thermal conductivity and thermal boundary resistance measurements of phase-change chalcogenides alloys

Jean-Luc Battaglia,[a]) 🆔 Andrzej Kusiak, and Kanka Ghosh 🆔

AFFILIATIONS

I2M Laboratory, UMR CNRS 5295, University of Bordeaux, 351 cours de la libération, 33400 Talence, France

Note: This paper is part of the Special Topic on Photothermics.
[a])**Author to whom correspondence should be addressed:** jean-luc.battaglia@u-bordeaux.fr

ABSTRACT

This article presents three photothermal methods dedicated to the measurement of the thermal properties of chalcogenide alloys, used as a central element in the new generations of non-volatile memory. These materials have two phases, amorphous and crystalline, possessing a sharp contrast in their electrical and thermal properties. In the crystalline phase, the properties also change very significantly with temperature. The control of the temperature of the samples, the choice of transducers, and the time or frequency characteristic values of the photothermal excitation are thoroughly discussed. Each photothermal technique is described from the experimental point of view as well as from the inverse method, performed to identify the parameters of interest. The identified thermal properties mainly concern the thermal conductivity and the thermal resistance at the interfaces between the phase-change materials and the materials in contact as encountered in the production of the microelectronic memory device. Assessing various photothermal techniques, the study suggests that pulsed photothermal radiometry is the most effective method for sensitive high-temperature measurements of thermal properties of the phase-change materials.

I. INTRODUCTION

The phase-change materials (PCMs) have been largely studied for several years because of their useful implementation within the field of non-volatile memories,[1–4] leading to the phase-change RAM or PCRAM. Those chalcogenide binary or ternary alloys involve at least one chalcogenide element, generally Te, and one or two other elements from columns 13, 14, and 15 as Ge, In, and Sb. The most well studied compounds are based on the In–Sb–Te and Ge–Sb–Te systems as reported in Fig. 1(a). These alloys are implemented in non-volatile memory devices because their electrical resistivity R_e varies across several decades, according to the crystalline state of the alloys as showed in Fig. 1(b). In the amorphous state, the electrical resistivity is high and the material behaves as an insulator, whereas in the crystalline state, the electrical resistivity is very low and the material behaves like a metal. A bit, whether 0 or 1 or even intermediate,[4,5] can be thus linked to this electrical state

of the alloy. A continuous scaling of PCRAM devices is well observed down-to the nanometer characteristic dimension[6–8] across years. Indeed, the technologies for the implementation of the alloy have not ceased to evolve over time in order to reduce the transition times for the phase change as well as the power consumption required for this change. Thus, the first technologies have relied on the thin layer technology, which leads to a variation in the so-called "mushroom" programming volume due to the shape of the half-sherry volume on the heating electrode.[9,10] More complex forms as micro-trenches have also emerged.[11] Finally, the latest developments aim to implement the phase-change material in the form of nanowires[12–14] whose diameter does not exceed a few nanometers or as PCM superlattices leading to the interfacial phase change memory technology.[15]

The thermal property measurement of PCM is a crucial step for their implementation in PCRAM.[16–18] Indeed, knowing both the thermal properties, as a function of the temperature, and the crystalline state will allow the calculation of the electrical power
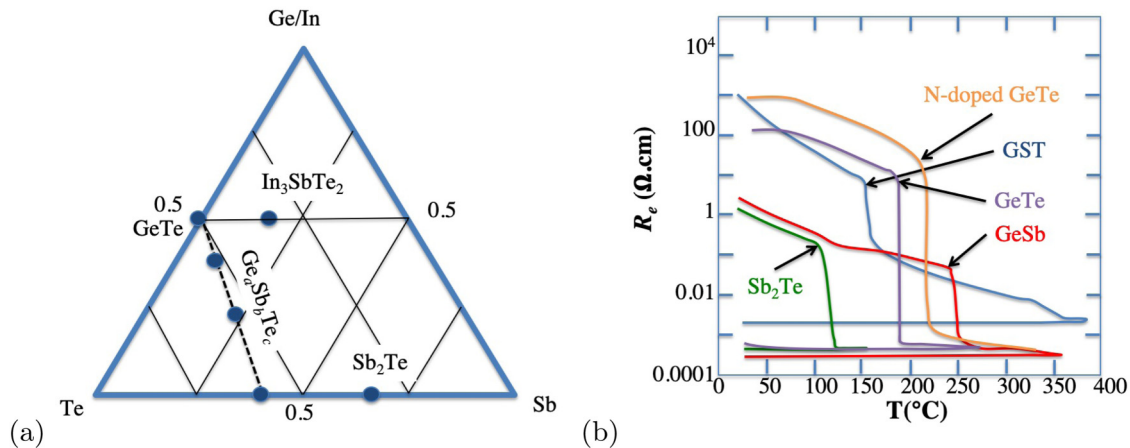
FIG. 1. (a) An overview of the phase-change alloys that have been investigated using the Ge–Sb–Te and In–Sb–Te ternary diagrams. (b) Resistivity as a function of temperature during a heating cycle for initially amorphous, as-deposited films of various phase-change materials (PCMs).

and associated transient waveform required for the phase change. In addition, it also allows for the design of the memory cell in order to avoid the thermal crosstalk effects with neighboring cells.[19,20] The measurement of PCM thermal conductivity must be performed over the entire temperature range including the amorphous-crystalline phase transition and up to the melting temperature. It is also well-established that the thermal boundary resistance (TBR) at the interfaces between the PCM microvolume and neighboring materials, such as the dielectrics and metal electrodes, has a comparable influence than that of the thermal conductivity on the heat transfer within the device.[19,21–23] It must be emphasized that, when the characteristic dimension of the system becomes comparable to or less than the average mean free path of the elementary heat carriers (phonons and electrons), the thermal conductivity has no longer physical meaning from the point of view of Fourier's law. In such a case, the measurement of the thermal resistance or conductance of these nanostructured materials is achievable. Typically, there are two major classes of methods for the thermal characterization of materials deposited in thin layers or nanostructured: contact methods and non-contact methods. Contact methods, as the 3ω[24–26] and the scanning thermal microscopy (SThM),[27–34] have the advantage of having absolute measurements of flux and temperature. The major drawback of the contact methods is the presence of the additional unknown parameters, relating to the contact itself and the significant thermal inertia of the probes, which introduce difficulties in processing the very fast transients.

In this paper, we will discuss the implementation of PTR techniques as the periodic (MPTR) and pulsed (PPTR) photothermal radiometry within the infrared (IR) and the time domain thermoreflectance (TDTR). All those PTR methods are based on the response to a thermal disturbance, generated as a heat flux $\varphi_0(t)$ at the surface of the investigated material. This disturbance must be small enough to fulfill the linearity requirement, regardless of the value of the initial temperature (T_i) of the material. The three

methods are complementary since they involve different characteristic time or frequency range by decades as well as different spatial resolution. First, we present all the technological solutions provided to carry out the temperature control of the sample. In particular, we show the influence of the thermal loading of the sample on this temperature control and on the choice of the most appropriate optical-to-thermal transducer. Second, we present the most efficient minimization techniques and more particularly show the contribution of inference techniques to predict the confidence domain of the parameters identified with greater accuracy. It must be noted that the inverse method is poorly discussed in the literature, whereas it constitutes a fundamental step towards finding the thermal properties, regarding mainly the identifiability of the unknown parameters based on a sensitivity study. On the other hand, the confidence domain of the identified parameters depends not only on the statistical properties of the measured signal but also on the minimization method used. Finally, the most advanced experimental configurations for MPTR, PPTR, and TDTR are presented, focusing on the laser excitation time waveform and the signal processing that involves both the model of the experiment and the inverse procedure. The model is sometimes restricted to the heat diffusion within the sample, whereas the complete acquisition chain affects the measured signal. A global model is thus required that accounts with the all the experimental parameters. The inverse method aims to minimize the difference between the measured physical quantity and its value calculated from the model discussed just before. The minimization is achieved by implementing a set of suitable mathematical methods whose literature is rich.[35] On the other hand, it is clear that thermal conductivity and TBR parameters are not always separately identifiable according to the experimental configuration. Therefore, specific strategies have to be implemented to separately distinguish TBR and thermal conductivity, which can be done using the sensitivity analysis. In addition, it must also be said that some sample configurations, such as thin films stacks or super lattices, also involve several interfaces,

and it is extremely difficult to identify them separately. A typical case for the PCRAM application is the stack formed by the metal electrode, the PCM layer, and the dielectrics material that ensures electrical and thermal insulation of the operating cell.

II. GENERAL CONSIDERATIONS

A. Controlling the sample temperature

The PCM layer is generally deposited on a Si wafer with SiO_2 thermal oxide at the surface. The adhesion of the PCM on SiO_2 is generally high and does not require an interfacial layer. Additional layers, including the optical-to-thermal transducer, have to be considered, and finally, a stack of thin layers is obtained. The sample is put inside a furnace that allows controlling the annealing temperature. The use of PTR methods requires the oven to be equipped with an appropriate window that allows the passage of the pump and probe laser for the methods based on thermoreflectance (TDTR), as well as the laser and the IR radiation for the radiometry methods (MPTR and PPTR). The designed furnace is represented in Fig. 2(a). The window is CaF_2 for MPTR and PPTR methods since it is transparent for both the visible and infrared radiation as showed in Fig. 2(a). For the TDTR method, the window is silica glass since the pump and probe lasers work within the visible wavelength as represented in Fig. 2(b). The silica glass transmittance according to the radiation wavelength is reported in Fig. 2(b).

There is no need for a perfect uniform temperature of the sample as long as it is stationary. The out-of-plane temperature gradient within the sample is low for low temperature, whereas it increases drastically as the temperature increases. Indeed, convection and even more radiation are enhanced as the temperature gap between the sample and the ambient is high. In addition, the contact between the sample and the furnace is very weak, leading to a high thermal resistance at the interface. For the MPTR and PPTR configurations, there is no benefice from the CaF_2 window

to make greenhouse to occur since transmittance is high within IR. It is then required performing a calibration of the sample surface temperature for each type of transducer used (see Sec. II B) since heat loss by radiation will depend on the emissivity of this material. An illustration is given in Fig. 3(b) considering a sample capped with a Pt layer. The emissivity of Pt is well measured[36] and varies according to wavelength and temperature as reported in Fig. 3(a). Such dependence makes absolute temperature measurement at the surface of the sample quite difficult. The second solution is to use the glass transition temperature [see Fig. 1(b)] of the PCM as fixed points on the experimental calibration curve. However, it must be noted that the crystallization temperature could vary with the film thickness when the former is low, typically of order of some nanometers. Therefore, the calibration with fixed points has to be performed considering thick PCM layers, in general, more than 100 nm. Both the fixed point and the calibration from surface temperature measurement are known, they are used simultaneously, which allows one to achieve a better accuracy. This calibration is not required anymore for the TDTR method since the silica glass window makes the greenhouse to occur, and it is then observed that the temperature at the sample surface is not significantly different from the set temperature of the furnace.

In order to limit the heat loss by convection and also the sample oxidation, one can implement a secondary vacuum within the furnace. However, given that it comes to lower the vaporization temperature of the transducer material, a continuous deposition of chemical species from the sample to the window of the oven is observed. This contributes to modify the structure of the layers and to obstruct the window at very short terms. A more efficient solution consists in producing a flow of argon gas within the oven enclosure.

For all the characterizations performed using either the MPTR, the PPTR, or the TDTR, the temperature ramp is 25 °C/min and the stabilization time is 2 min. The measurement
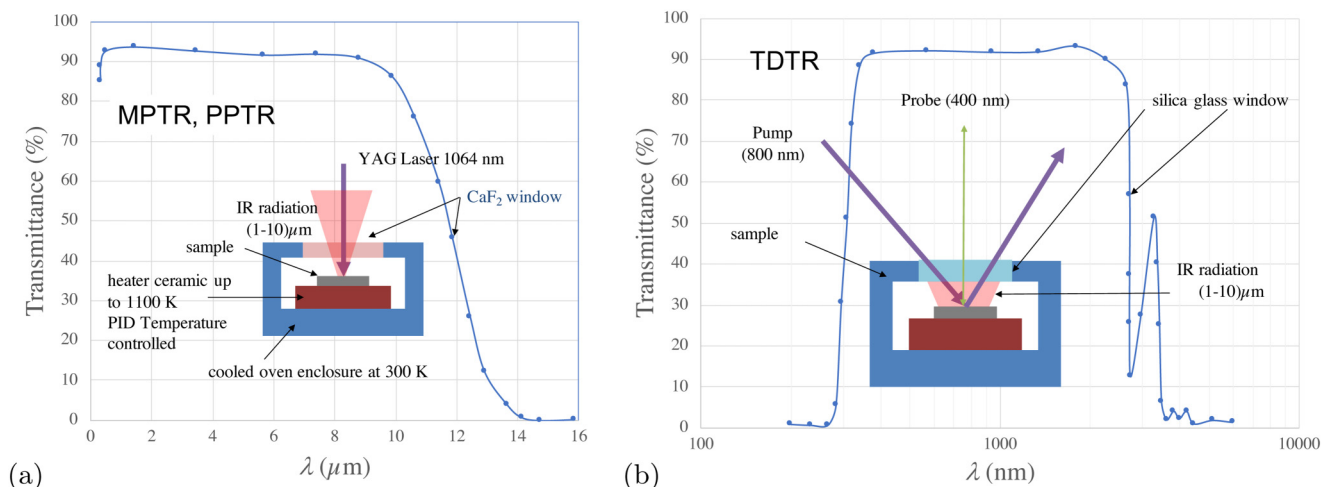

FIG. 2. (a) Designed furnace for the MPTR and PPTR methods at temperature up to 1100 K; CaF_2 transmittance within the visible and IR wavelength range; (b) designed furnace for the TDTR method (transmittance of silica glass within the visible and IR wavelength range).
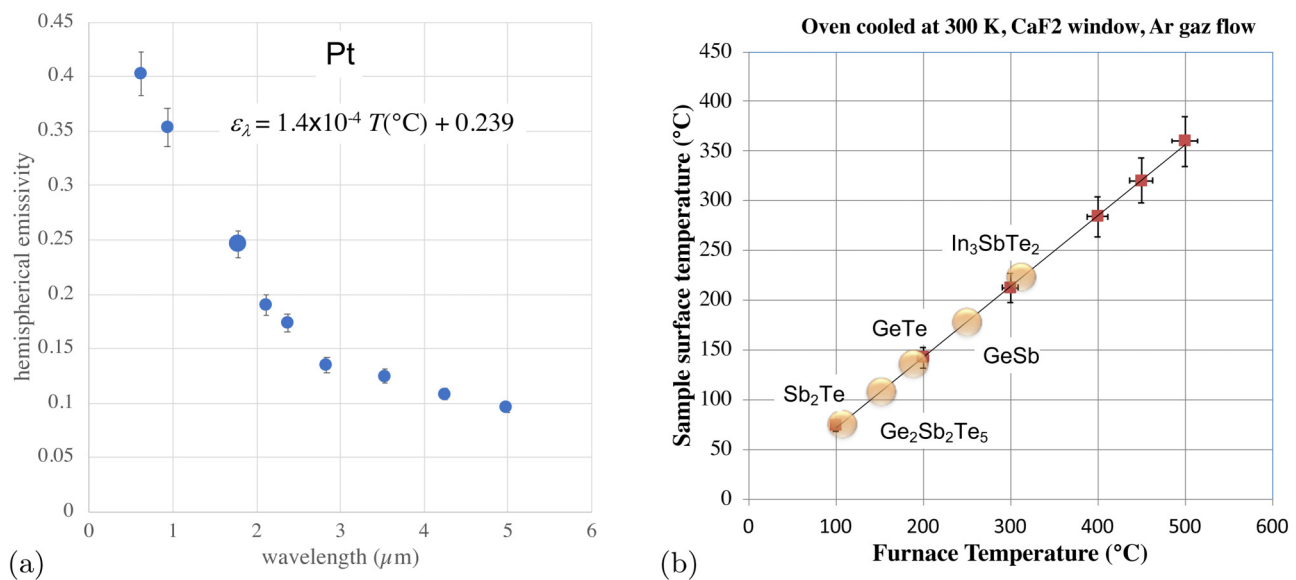
FIG. 3. (a) Pt spectral hemispherical emissivity according to wavelength and temperature; (b) surface temperature of the sample measured using an IR camera. The oven enclosure is cooled at 300 K, there is a flow of Ar gas within the furnace and the window is CaF_2. Crystallization temperature of different thick PCM alloys are reported on the plot.

time is about 10 min at each investigated temperature for the MPTR and TDTR methods, whereas it is only about 20 s for the PPTR one.

B. Optical-to-thermal transducer

The alloys constituting the PCMs are generally transparent to the wavelength of the laser, regardless of the choice of the PTR method. A full volume absorption does not make it possible to generate a temperature gradient within the layer to be characterized and, therefore, to reach its thermal conductivity. On the other hand, the PCM alloys being semiconductors, the carrier response is very easily observed during the passage of the bandgap within the IR signal. Thus, in order to control the absorption of the laser at the surface of the material, it is common to deposit a layer, called optical-to-thermal transducer whose role is to transform the incident photons into a surface heat flux. It must be said that the literature is often very discrete regarding the choice of the material transducer for high-temperature characterization as well as its thickness value. Most of the studies do not make a physicochemical investigation of the layers as well as their interfaces after the application of the high-temperature budget. The TiN material would be very effective for high-temperature application, and it would be also very interesting since it is generally used as the metal electrodes within the PCRAM device. Unfortunately, this material is not opaque within the visible wavelength. For MPTR and PPTR radiometry techniques in the IR, it is strongly advised to search for a transducer whose properties come closest to a blackbody. Unfortunately, many candidate materials do not withstand high temperatures. For instance, chromium is an excellent candidate for

low temperatures given its high emission factor in IR. However, when the temperature reaches 300 °C, cracks are observed on the surface of the sample. After testing several coating layers, we found that the only material that can withstand high-temperature levels, without evaporating nor oxidizing, is platinum. However, as showed in Fig. 3(a) the properties of platinum for both the absorption in the visible wavelength and the emission within the IR are low. As reported in Fig. 4(a), Time of Flight-Secondary Ion Mass Spectrometry (ToF-SIMS) has been performed at room temperature (RT) for a 30 nm thick Pt layer deposited on a 210 nm amorphous GeSbTe thick layer. The measurement was then done for the annealed sample at 400 °C when the PCM phase change has been reached. It is thus observed a slightly diffusion of Pt within the $Ge_2Sb_2Te_5$ (GST) layer close to the interface. This observation leads to limit the use of this technique to layers whose thickness is large enough (more than 100 nm in practice) in order to not be significantly affected by the transducer material diffusion at high temperature. We also observed that the diffusion of species between platinum and most chalcogen alloys (GeTe, SbTe, InSb, InSbTe) remained very limited. It is obviously recommended to limit the duration of the thermal budget of the investigated samples during the experiment by carefully choosing the temperature ramp as well as the duration of the measurement at each scanned temperature.

For thermoreflectance, we look for a material whose reflectivity as a function of the temperature is large. Pt is not suited for such measurement and Au diffuses very quickly within the PCM alloys as soon as the temperature increases. Al is generally the material that presents satisfying properties in terms of temperature dependent reflectivity and that can withstand thermal budget as high as 400 °C at the maximum without apparition of visible
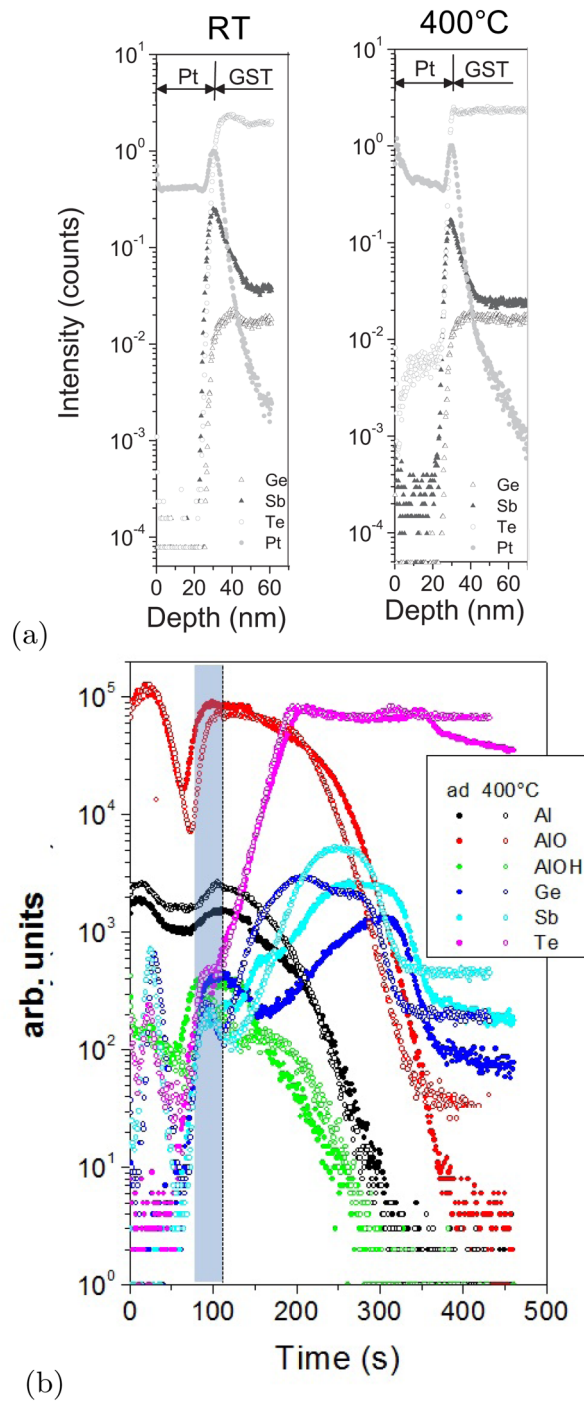
(a)

(b)

FIG. 4. (a) ToF-SIMS for the as-deposited amorphous GST with Pt capped layer and the annealed sample at 400 °C (GST in the *hcp* phase);[37] (b) ToF-SIMS for the as-deposited (ad) amorphous GST with the Al capped layer and the annealed sample at 400 °C (GST in the *hcp* phase).[38] The dashed line locates the perfectly flat ideal interface, and the gray area evidenced the interface width.

surface degradation. However, ToF-SIMS performed on amorphous and 400 °C annealed sample evidences changes in depth profiles for Ge, Sb, and Te species with diffusion into the Al layer and up to the Al surface after annealing [Fig. 4(b)]. There is no Al diffusion into GST, the apparent higher intensity seen in the annealed sample being due to the concomitant Ge, Sb, Te diffusion at the interface. Both information regarding surface roughness and mass diffusion allow us defining the interface layer to be 0.9–3 nm thick. Moreover, roughness uniformity allows us to conclude that the mass amounts of GST and Al in the interface layer are close to $\beta = 60\%$ and $(1 - \beta) = 40\%$, respectively. This also leads us to conclude that the method should be used for PCM layer whose thickness is higher than 100 nm.

A fundamental comment is about the fact that the thermal budget applied to the sample for the characterization is far from the way the PCM is heated during the PCRAM device operation. This has not been clearly studied but the thermal load operation will significantly change the way the interface is modified over time. In the same vein, it is important to note that all the thermal characterization experimental procedure reported in the literature omit to specify the conditions of thermal load of the PCM materials. Therefore, the thermal resistance measurement at the interfaces between the PCM and neighbored layers reported within the literature has to be considered with high caution.

C. Investigated depth within the sample

When the heat flux is a periodic function of time with angular frequency $\omega = 2\pi f$ (MPTR), the thermal diffusion length within the expected material is a function of its thermal diffusivity a, that is the ratio $k/\rho C_p$ of the thermal conductivity and the specific heat per unit volume, and the frequency f as: $z_h = \sqrt{a/\pi f}$. Similarly, when the heat flux is generated as a pulse with duration τ (PPTR, TDTR), the minimum investigated depth within the material is $z_{h,min} = \sqrt{a\tau}$. The typical heat penetration depth is illustrated in
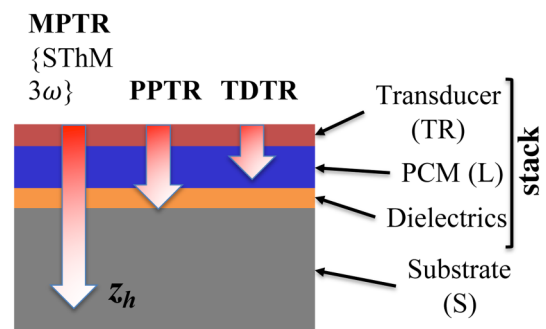

FIG. 5. The investigated heat penetration depth within the sample according to the technique used. The transducer thickness depends on the temperature range swept during the characterization, i.e., at ambient measurement the thickness transducer can be small enough (10 nm), whereas it must be larger at high temperature (100 nm) in order to resist to both thermomechanical constraints and evaporation. The 3ω and SThM techniques are also reported for information. Some additional interfacial layers can be considered with regard to adhesion purpose of the transducer.

TABLE I. R_T: thermal resistance involved within the heat transfer model considering the stack deposited on the substrate (S) and capped with the transducer (TR) as represented in Fig. 5; t_l and k_l are the thickness and the thermal conductivity of the PCM layer (L); R_K is the intrinsic thermal resistances for the layers (TR and D) involved in the stacks with known thermal conductivity; TBR_i denotes the thermal resistance at each interface i within the stack; Θ is the vector of identified parameters using the NLSQ method, **P** is the vector of identified parameters including uncertainties on known parameters using the Markov Chain Monte Carlo (MCMC) method (see the related section for the description of those experimental parameters).

Method	R_T	Θ	**P**
MPTR	$t_l/k_l + R_K + R_c$, with $R_K = \sum_i t_i/k_i$ and $R_c = \sum_i TBR_i$	R_T [k_l and R_c if $R_T = f(t_l)$ available]	$\Theta + \{r_0, r_d, R_K, a_s, k_s\} + \{\phi_{det}\}$ (see Sec. III A)
PPTR and TDTR	$R_c + t_l/k_l$, with $R_c = TBR(TR/L)$	k_l, R_c	$\Theta + \{t_l\} + \{f_m, f_{cut}, t_{del}\}$ for the PPTR (see Sec. III C) $\Theta + \{f_m\}$ for the TDTR (see Sec. III B)

Fig. 5, considering the three different methods. The thickness of the layers constitutive of the stack being of the order of some tenth of nanometers, only the thermal resistance of the investigated stack deposited on the substrate can be reached by using the MPTR. This thermal resistance includes both the intrinsic thermal resistance t/k of the layers from the stack and the sum R_c of the TBR at the interfaces between the layers. A very important point in the use of the experimental data for this technique is that here the substrate defines the reference for these measurements since only the relative variations of temperature can be measured. It is, therefore, important to know the thermal properties of the substrate, over the entire temperature range explored, with great accuracy. For the PPTR and TDTR, it is expected that the thermal conductivity of the layer as well as the TBR can be identified separately. Nevertheless, for these two methods which lead to the measurement of the relative temperature variation, it is the transducer that constitutes the reference with respect to the use of the experimental data with regard to the model. The properties of the transducers must, therefore, be known with precision over the entire temperature range explored for these two methods. Table I presents the parameters that can be identified for the three methods. The three methods, therefore, appear to be complementary because they lead to different information but which, in fine, must overlap and lead, in particular, to the different values of thermal conductivity of the PCM and of the thermal resistances at the different interfaces.

D. Identification procedure

The identification of the seek parameters $\Theta = [\alpha_i]$ (α_i being either a thermal resistance, a thermal conductivity, a TBR, or other unknown parameters related to the experimental configuration used) is based on several mathematical algorithms. The two most appropriate classes of methods for this kind of inverse problem are the linear and nonlinear least square (LSQ, NLSQ) techniques and the Bayesian ones.[35] Of course, other techniques can be used (genetic algorithms, particle swarm, etc.), but they will not provide additional information than those obtained by the two classes of methods mentioned above. Within the first class (as Newton–Gauss, Levenberg–Marquardt,[39] or trust-region-reflective algorithms[40]), the method will lead to minimize the quadratic gap between the experimental data and those calculated using a model of the heat transfer within the experimental configuration. If the sensitivity functions $S_Q(\alpha_i) = \partial Q/\partial \alpha_i$ of parameters α_i relative to the measured quantity Q (that is generally an absolute

relative temperature or a phase-lag) are linearly independent, the minimization of $J = \|\mathbf{Y} - \mathbf{Q}\|_2$, where $\mathbf{Q} = [\mathbf{Q}]_\mathbf{N}$ is the measurement vector constituted from N data, leads to a global minimum and then to the optimal values for α_i. On the other hand, this method allows estimating the standard deviation of the identified values using the covariance matrix for α_i at the end of the iterative minimization process and the residuals $\mathbf{E} = \mathbf{Y} - \mathbf{Q}$ that are expected to be comparable to the noise measurement assuming the model is unbiased. The covariance matrix is $\mathbf{cov}(\Theta) = (\mathbf{S}^T\mathbf{S})^{-1}$, where vector $\mathbf{S} = [S_Q(\alpha_i)]_\mathbf{N}$. It comes that the standard deviation of the identified parameters is $\sigma(\alpha_i|Y)^2 \sim \mathbf{cov}(\Theta)\mathbf{E}/\sqrt{N}$. The main advantage of the non-linear least square technique is the computation speed that is very fast when approaching the minimum. The drawback of this approach is that it assumes that other experimental parameters are known accurately, which is not true in practice. Some uncertainties can be put on the known parameters within the NLSQ technique assuming strong conditions. Therefore, the Bayesian minimization technique can be efficiently implemented assuming a standard deviation on the known parameters. Indeed, in this method, all variables involved in the model, formally gathered in column vector $\mathbf{P}$ ($\Theta \subset P$), are considered random variables. Information on variables is expressed as probability distributions. Each time a new information occurs for variables, it is combined with the previously available information through the Bayes's theorem, $\pi_{posterior}(\mathbf{P}) = \pi(\mathbf{P}|\mathbf{Y}) = \pi_{prior}(\mathbf{P})\pi(\mathbf{Y}|\mathbf{P})/\pi(\mathbf{Y})$, where $\pi_{posterior}(\mathbf{P})$ is the posterior probability density, that is, the conditional probability of the parameters $\mathbf{P}$ given the measurements $\mathbf{Y}$; $\pi_{prior}(\mathbf{P})$ is the prior density, that is, the coded information about the parameters prior to the measurements; $\pi(\mathbf{Y}|\mathbf{P})$ is the likelihood function, which expresses the likelihood of different measurement outcomes $\mathbf{Y}$ with $\mathbf{P}$ given; and $\pi(\mathbf{Y})$ is the marginal probability density of the measurements, which plays the role of a normalizing constant. This technique is generally implemented as a Markov Chain Monte Carlo method, known as the Metropolis–Hastings algorithm,[41] so that inference on the posterior probability becomes inference on the samples.

III. EXPERIMENTAL TECHNIQUES

A. The MPTR technique

The modulated photothermal radiometry method is a contactless measurement technique based on monitoring the emitted infrared radiation from the surface of the sample consequently to a periodic photothermal excitation $\varphi(t)$ provided by a laser.
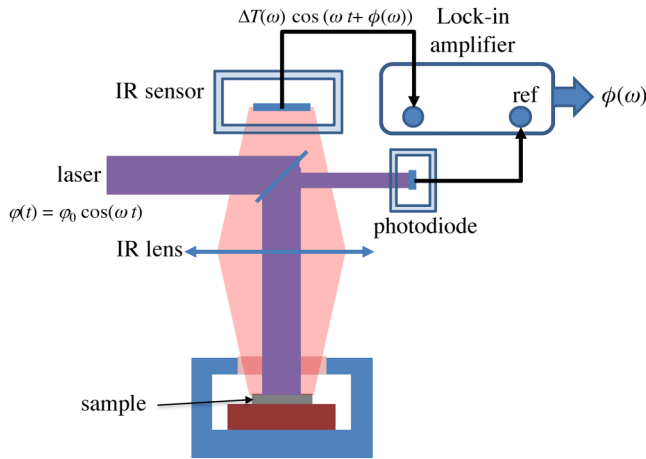
FIG. 6. The MPTR experimental setup.

Originally proposed in 1979,[42,43] the method has been extensively improved for both the experimental[44–46] and theoretical[47–52] aspects. The spatial distribution of the excitation can be uniform or with more complex form (Gaussian, for example). The radiation from the laser is absorbed by the surface of the sample, if opaque, leading to a surface heat flux φ. This results in an increase $\triangle T$ at the heating area leading to an infrared emitted radiation. Considering a periodic heat flux $\varphi(t) = \varphi_0 \cos(\omega t)$, the average temperature increase over the measurement area at the surface of the sample is constituted from a continuous and transient parts as: $\triangle T(t) = \triangle T_0 + \triangle T_\omega \cos(\omega t + \phi)$. Assuming small temperature increase, the transient part of the emitted radiation from the aimed area can be linearized as: $\triangle M = 4 \varepsilon \sigma_s \triangle T_0^3 \triangle T_\omega$. The sketch of the MPTR setup is presented in Fig. 6. A lock-in amplifier is used to measure the signal at the IR detector and leads to the amplitude $A(\omega)$ and phase-lag $\phi(\omega)$ measurements. As said previously, for thin layers of micrometer or sub-micrometer thickness deposited on a substrate, the MPTR allows measuring, as for the 3ω method, the global thermal resistance R_T of the deposit. The calibration of the amplitude vs the surface temperature requires knowing accurately the surface emissivity ε that comes to be a difficult task. Since the phase $\phi(\omega)$ is very sensitive to the thermal resistance of the layer, this measurement is used within the identification process. The average temperature over the aimed area at the surface of the sample is

$$\overline{\triangle T}(\omega) = \varphi_0 (Z_\infty(\omega) + R_T), \qquad (1)$$

with

$$Z_\infty(\omega) = \frac{r_0^2}{k_s \, r_d} \sum_{n=0}^{M} \frac{J_1(\alpha_n r_d) e^{-\left(\frac{\alpha_n r_0}{2}\right)^2}}{\alpha_n^2 \tanh\left(\sqrt{\alpha_n^2 + \frac{j\omega}{a_s}} e_t\right) \sqrt{\alpha_n^2 + \frac{j\omega}{a_s}} R^2 J_0(\alpha_n R)^2} \qquad (2)$$

and $\alpha_0 = 0$, $\alpha_n R = \pi(n + 1/4) - 3/(8\pi(n + 1/4))$ $(n > 0)$, r_0 is the laser beam radius, r_d is the radius of the aimed area by the IR detector, k_s and a_s are, respectively, the thermal conductivity and thermal diffusivity of the substrate with thickness e_t [for a semi-infinite behavior $\tanh(\infty) = 1$]. Finally, J_0 and J_1 are the first kind Bessel functions of 0 and 1 order, respectively. The phase-lag is then $\phi(\omega) = \arg \overline{\triangle T}(\omega) = \arctan\left(\mathrm{Im}(\overline{\triangle T}(\omega))/\mathrm{Re}(\overline{\triangle T}(\omega))\right)$. The detector and associated amplifier involve a phase-lag ϕ_{det} that increases linearly with the frequency ω. The function $\phi_{det}(\omega)$ has to be calibrated using a fast IR led and the model for the phase is, therefore, $\widetilde{\phi}(\omega) = \phi(\omega) + \phi_{det}(\omega)$. Considering the measured value $Y_\phi(\omega_i)$ of the phase-lag at different frequency ω_i $(i = 1, N)$, the objective function is $J = \left\| \mathbf{Y_\phi} - \mathbf{\Psi} \right\|_2$, where $\mathbf{Y_\phi} = Y_\phi(\omega_i)$ and $\mathbf{\Psi} = \widetilde{\phi}(\omega_i)$ are respectively the measured and simulated phase at all the investigated frequencies. The value of R_T can be identified using a nonlinear least square (NLSQ) technique as the Newton–Gauss or Levenberg–Marquardt algorithm. In that case, the standard deviation on R_T is achieved from the covariance matrix at the end of the iterative process. In order to introduce uncertainties on geometrical properties as e_t, r_0, and r_d as well on the substrate thermal properties a_s and k_s and the phase-lag ϕ_{det} of the detector it is recommended to use the Markov Chain Monte Carlo (MCMC) method with appropriate variations. As described in Table I, the thermal resistance R_T includes the intrinsic thermal conductivity k_l of the PCM layer (L) as well as the thermal resistance of other layers (TR and D) constituting the stack presented in Fig. 5, and finally, the sum R_c of the thermal resistances at the interfaces between layers of the stack. The MPTR allow the determination of R_T and that of k_l and R_c if the experiment can be repeated with different values of the thickness t_l. In such a case, a linear regression is applied to the resistance measurements as a function of the thickness for each temperature of the PCM that leads to the value of the two parameters ($1/k_l$ being the slope and R_c the value at the origin). This approach has the advantage of increasing the accuracy of the measurement on the two parameters by confirming a linearity relationship. The major drawback remains the obligation to fabricate additional samples and the duration of the characterization experiments also becomes much longer.

The method has been used to measure the temperature dependent thermal conductivity of several chalcogenide alloys: $Ge_2Sb_2Te_5$ (GST),[37] GeTe,[53] C-doped GeTe,[54] and $In_3Sb_1Te_2$.[55] It has been also used to investigate the TBR at the SiO_2–GST interface[37] and the role of Ti at the interface between TiN (the metal electrode in the PCRAM) and GST.[56]

B. The TDTR technique

Originally designed to study ultrafast phenomena, the time domain thermoreflectance (TDTR) has been implemented within the framework of thermal characterization.[57] The technique has been largely improved up to nowadays.[58–60] A high-energy picoseconds or even femtoseconds laser produces a very short pulse with high frequency repetition rate f_m. The beam is split as a low-energy probe beam and a high-energy pump beam. Pump and probe beams have generally the same diameter and are superimposed at the sample surface. Drawbacks in using a mechanical stage as the optical delay line can be avoided by using the heterodyne

method.[61] The pump is modulated at a low frequency that allows the accurate extraction of the measured periodic change of surface reflectivity using a lock-in amplifier that measure the voltage drop at the photodiode. The probe is continuously delayed from the pump with time τ in the nanoseconds time range. The pump is thus used to heat the sample surface, whereas the probe is used to monitor the change of surface reflectivity $\Delta R/R_0$ using a photodiode. Assuming this change is proportional to that of the temperature, it is then obtained the quantity of interest for the identification process (Fig. 7).

An optical-to-thermal transducer is used that is generally gold or aluminum. The diameter of the pump is larger than the PCM film thickness leading to consider one-dimensional heat diffusion within the sample. On the other hand, given to the very fast transient excitation and observation time, the TDTR method leads to exploring only the PCM layer and the interface with the transducer layer. The model that allows to simulate the measured signal by the lock-in has to account also with the modulation of the laser beam, and it is finally obtained

$$D(t) = \sum_{n=-\infty}^{+\infty} \overline{\triangle T}\left(2\pi\left(\frac{n}{\tau}+f_m\right)\right) \exp\left(-\frac{j2\pi n t}{f_m}\right). \quad (3)$$

Assuming the transducer thickness is small enough to consider the layer at a uniform temperature at each time, one has

$$\overline{\triangle T}(\omega) = \varphi_0\left(1/E_l\sqrt{j\omega} + R_T\right), \quad (4)$$

where $E_l = \sqrt{k_l \rho_l C_{p,l}}$ is the effusivity of the PCM layer. Since the heat flux absorbed by the surface from the pump is not known in practice and that it is only measured a relative variation of the temperature at the surface, a normalized function $\widetilde{D}(t)$ of $D(t)$ with respect to its value at t chosen between 0 and τ is considered. Both R_T and k_l can be identified using either the NLSQ or the MCMC
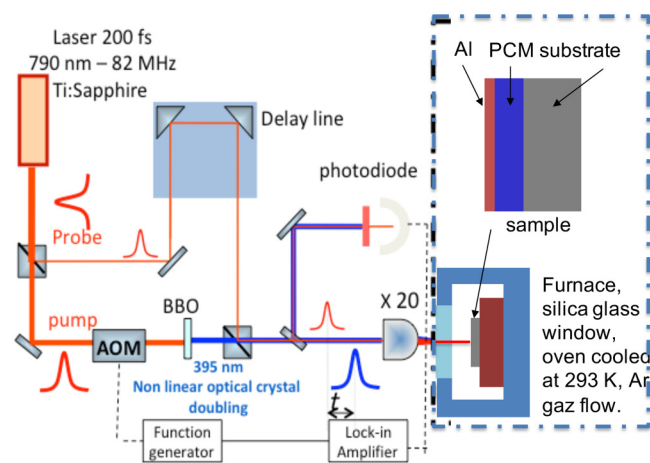
technique, although the former is recommended in order to introduce an uncertainty on the modulation frequency f_m.

The method has been used to measure the temperature dependent thermal conductivity of several PCMs, GST,[62–64] Sb_2Te_3,[65] and GeTe.[66] It has been also used to measure the TBR at the GST–Al interface,[38] the TBR at the TiN–GST interface[21,23,67] and the influence of fullerene C_{60} at the GST–TiN interface.[68]

Unfortunately, the material used as the transducer (Al or Au) are not suited to work at high temperature, the maximum admissible temperature being of the order of 300 °C, beyond which cracking as well as a strong atomic diffusion is observed. Given that we are seeking to develop PCMs with a high crystallization temperature for high-temperature applications, the TDTR method turns out to be less and less suitable for this type of characterization.

C. The front face PPTR technique

The approach is similar to that of the MPTR but in that case the photothermal source is continuously emitting nanoseconds heat pulses at frequency f_m ranging from 1 kHz up to 100 kHz. Once the steady periodic regime is reached, the signal measured by the IR detector, which is proportional to the front face temperature, is recorded after every pulses and averaged with the previous average signal. In comparison with the classical flash technique,[69] and even accounting with all the successive improvements,[70–78] averaging the recorded signal leads to a significant improvement of the signal noise ratio[79] since the standard deviation of measured values of noise is reduced by $\sqrt{N_s}$, where N_s denotes the number of pulses used to perform the average. A fast IR detector (20 MHz and nanoseconds rise time) is implemented. The optical arrangement is quite similar to that of the MPTR in order to make the image of the sensitive element of the detector on the heated area by the laser. The sketch of the experimental setup is represented in Fig. 8.

Accounting with the periodic repetition, it is obtained that the signal measured between two successive pulses, when the stationary regime is reached, is expressed from the average temperature on the
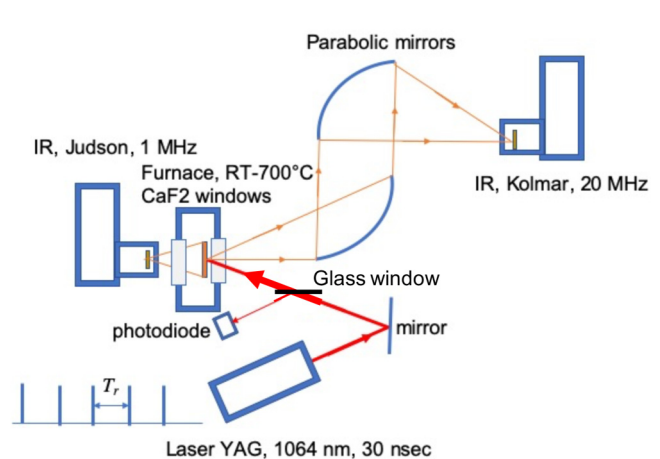

FIG. 7. Sketch of TDTR experimental setup.

FIG. 8. Sketch of the PPTR experimental setup.

aimed area as

$$D(t) = \sum_{n=-\infty}^{+\infty} \overline{\triangle T}(2\pi f_m) \, \exp\left(-\frac{j\,2\,\pi\,n\,t}{f_m}\right). \qquad (5)$$

If the layer behaves as a semi-infinite medium for the value of f_m, meaning $e_l \gg \sqrt{a_l/\pi f_m}$, then $\overline{\triangle T}(\omega)$ is given by relation (1) with $\tanh(\infty) = 1$ and replacing k_s and a_s by the properties of the layer, i.e., k_l and a_l. The thermal resistance $R_T = e_{TR}/k_{TR} + R_c$ is the sum of the intrinsic resistance of the transducer layer with the contact resistance R_c at the interface between the transducer and the PCM layer. Since the laser beam radius is much large than the layer thickness, the heat transfer is one dimensional and the relation (1) can be simplified to obtain the same expression of $\overline{\triangle T}(\omega)$ than that of the TDTR technique, e.g., relation (4). Hence, E and R_T can be identified using the minimization algorithms discussed below. In case, the heat penetration depth is larger than the PCM layer thickness but still less that the laser beam radius, a model based on the thermal impedance network method[80] can be implemented.

Regarding the sample configuration, the network is as the one represented in Fig. 9 with $Z_1(\omega) = (\cosh(\beta e_I) - 1)/(k_l\beta \sinh(\beta e_I))$, $Z_3(\omega) = 1/(k_l\beta \sinh(\beta e_I))$, $\beta = \sqrt{j\omega/a_l}$, $E_s = \sqrt{k_s\rho_s C_{p,s}}$, and $Z_s(\omega) = 1/E_s \sqrt{j\omega}$. Therefore, the temperature at the aimed area is

$$\overline{\triangle T}(\omega) = \varphi_0 \left(\frac{1}{\frac{1}{Z_3(\omega)} + \frac{1}{Z_1(\omega)+Z_s(\omega)}} + Z_1(\omega) + R_T \right). \qquad (6)$$

Since the heat flux absorbed by the surface from the laser is not known in practice and that it is only measured a relative variation of the temperature at the surface, a normalized function $\widetilde{D}(t)$ of $D(t)$ with respect to its value at t chosen between 0 and $1/f_m$ is considered. The model has to account with the frequency transforms $H_\varphi(\omega)$ of the pulse transient waveform and the transfer function $H_{det}(\omega)$ of the detector that is considered as a delayed first-order low-pass filter with cut-off frequency f_{cut} and delay t_{del}. It leads to replace $\overline{\triangle T}(\omega)$ by the double convolution product $\overline{\triangle T}(\omega)*H_\varphi(\omega)*H_{det}(\omega)$.

Both R_T and k_l can be identified using the NLSQ algorithm, although it is rather recommended to use the Bayesian technique, which allows introducing uncertainties on $\{t_l, f_m, f_{cut}, t_{del}\}$. The
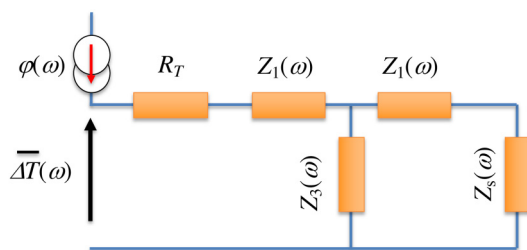

FIG. 9. Heat transfer model within the front face PPTR configuration considering the heat penetration depth is larger than the PCM thickness.

PPTR method has advantages for the characterization of high-temperature PCM layers. The first is that the sensitivity of the method remains two orders of magnitude above that based on thermo-reflectivity. The second is the possibility of using transducers whose chemical affinity with PCMs is low (as Pt) and which resist well at high temperatures, at least up to 500 °C. Finally, the method, in its current state, makes it possible to explore layers of a few tenths to hundred nanometers without the contact with the lower layers being considered. Considerable technological progress now makes it possible to use detectors whose acquisition frequency can reach 100 MHz. This is still insufficient to compete with the TDTR method, but it will make it possible to characterize layers of PCM of a few tens of nanometers without having to diffuse into the lower layers. It, therefore, seems that real progress can be obtained by using the PPTR method for the characterization of thin layers of PCM as a function of temperature in the future. The method is quite recent and has been only used to measure the thermal conductivity of the amorphous GeTe alloy and the TBR at the interface with Pt.[81]

IV. ILLUSTRATIONS

We give in Fig. 10 the results obtained by using the three methods described previously for three phase-change alloys, namely, $Ge_2Sb_2Te_5$ (GST), $In_3Sb_1Te_2$ (IST), and GeTe. The PPTR method was used for GeTe, the MPTR method was used for the IST and the TDTR method was used for the GST. For each alloy, we start from the amorphous state and we perform a measurement for each prescribed temperature of the sample. The standard deviation for each identified value is also reported in the figure, and it must be also accounted with the 5% of uncertainty for the annealed temperature of the sample (only represented for GeTe in the figure) As one might expect, the thermal conductivity of materials in the amorphous state does not change with temperature. Then, we observe for the three systems a glass transition to the crystalline
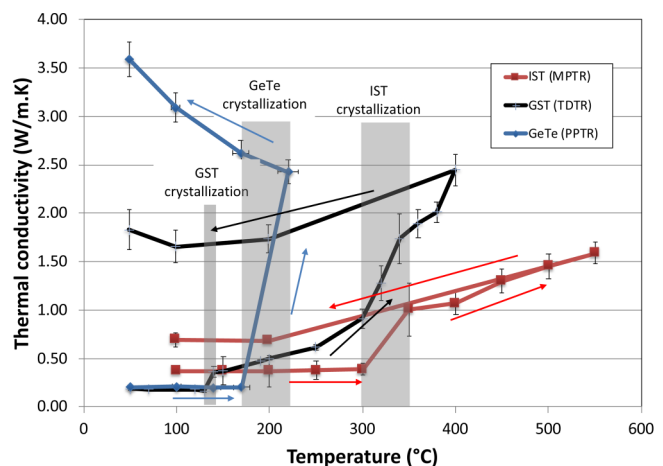

FIG. 10. Illustration of the use of the three techniques for the thermal conductivity measurement of $Ge_2Sb_2Te_5$ (GST), $In_3Sb_1Te_2$ (IST), and GeTe.

state as well as a variation of the conductivity of the crystalline phase with the temperature, the slope of which being essentially linked to the electronic behavior. These variations are in agreement with the electrical resistivity measurements as we presented them in Fig. 1(b) in the Introduction section. A mainly striking result is above all the uncertainty on the glass transition temperature T_c value, which is within the shaded areas in the figure. In fact, the amorphous phase being very unstable, the transition to the crystalline state may appear during a measurement at a temperature slightly below T_c, whatever the technique used. For information the exact phase change temperature are $150\,°C$ for GST, $180\,°C$ for GeTe, and $320\,°C$ for IST. It is, therefore, essential to carry out the measurement, at a given temperature, in the shortest possible time in order to minimize the transition from the amorphous state to the crystalline state when one approaches the transition. It should also be noted that the shorter the thermal loading time, the more the risks of degradation of the transducers, as well as the diffusion of species between layers are minimized. The PPTR method is the most efficient for this purpose since only one transient measurement is required at a given temperature, while the MPTR and TDTR methods require several.

V. CONCLUSION

In this paper, we proposed a review of the latest developments achieved for three photothermal radiometry methods used for the measurement of thermal properties as the thermal conductivity of phase-change chalcogenide alloys and related thermal boundary resistances. Those methods are complementary not only in terms of improving the accuracy of the seek parameters but also to discriminate easily the thermal resistance at the interfaces between the PCM and the adjacent layers that are the metallic dielectrics and electrodes of the PCRAM cell. As we have shown, these methods are much more effective than contact methods (3ω and SThM) when we want to measure the changes in these thermal properties at high temperatures, above the phase-change temperature. We have particularly emphasized in this paper on the aspects linked to the implementation of devices for controlling the temperature of the sample, the choice of optical-thermal transducers, and the evolution of materials as a function of temperature. A conclusion to this part is that the thermal budget undergone by the samples will have a significant role on the evolution of the sample and in fact on the thermal properties. For fairly thick layers of the PCM, this especially has repercussions on the value of the TBR, given the strong interface variables which are observed in terms of composition and equivalent thickness. This also suggests that a thermal characterization of thin layers of PCM at high temperature should systematically be preceded and followed by a physicochemical characterization (ToF-SIMS, Raman, DRX), which takes account of the possible modifications undergone by the sample. This is still too rarely done systematically in most published studies on PCM. We have also shown the utility of using techniques for identifying unknown parameters which take into account the uncertainty on all the other known parameters, whether they are related to the experimental method or to the properties of materials, other than the PCM, constituting the sample. In this, the MCMC method is in our opinion the most efficient. Finally, we have shown that the PPTR technique becomes a credible alternative to the TDTR method for high temperatures where transducer materials have to withstand intense thermal loads. Further improvement is needed in this area so that the observation times allow an investigation of the PCM layer alone. However, recent technological developments to make IR detectors capable of operating at frequencies above 100 MHz can further open up avenues of real applications.

AUTHORS' CONTRIBUTIONS

All authors contributed equally to this work.

ACKNOWLEDGMENTS

DATA AVAILABILITY

The data that support the findings of this study are available within the article.

REFERENCES

[1] S. R. Ovshinsky, Phys. Rev. Lett. **21**, 1450 (1968).

[2] N. Yamada, E. Ohno, K. Nishiuchi, N. Akahira, and M. Takao, J. Appl. Phys. **69**, 2849 (1991).

[3] D. Lencer, M. Salinga, B. Grabowski, T. Hickel, J. Neugebauer, and M. Wuttig, Nat. Mater. **7**, 972 (2008).

[4] S. Raoux, F. Xiong, M. Wuttig, and E. Pop, MRS Bull. **39**, 703 (2014).

[5] W. Zhang, R. Mazzarello, M. Wuttig, and E. Ma, Nat. Rev. Mater. **4**, 150 (2019).

[6] A. Pirovano, A. L. Lacaita, A. Benvenuti, F. Pellizzer, S. Hudgens, and R. Bez, in *IEEE International Electron Devices Meeting 2003* (IEEE, 2003), pp. 29.6.1–29.6.4.

[7] S. Raoux, G. W. Burr, M. J. Breitwisch, C. T. Rettner, Y. Chen, R. M. Shelby, M. Salinga, D. Krebs, S. Chen, H. Lung, and C. H. Lam, IBM J. Res. Dev. **52**, 465 (2008).

[8] R. Annunziata, P. Zuliani, M. Borghi, G. De Sandre, L. Scotti, C. Prelini, M. Tosi, I. Tortorelli, and F. Pellizzer, in *2009 IEEE International Electron Devices Meeting (IEDM)* (IEEE, 2009), pp. 1–4.

[9] J. H. Yi, Y. H. Ha, J. H. Park, B. J. Kuh, H. Horii, Y. T. Kim, S. O. Park, Y. N. Hwang, S. H. Lee, S. J. Ahn, S. Y. Lee, J. S. Hong, K. H. Lee, N. I. Lee, H. K. Kang, U.-I. Chung, and J. T. Moon, in *IEEE International Electron Devices Meeting 2003* (IEEE, 2003), pp. 37.3.1–37.3.4.

[10] S. Tyson, G. Wicker, T. Lowrey, S. Hudgens, and K. Hunt, in *2000 IEEE Aerospace Conference. Proceedings (Cat. No.00TH8484)* (IEEE, 2000), Vol. 5, pp. 385–390.

[11] F. Pellizzer, A. Pirovanc, F. Ottogalli, M. Magistretti, M. Scaravaggi, P. Zuliani, M. Tosi, A. Benvenuti, P. Besana, S. Cadeo, T. Marangon, R. Morandi, R. Piva, A. Spandre, R. Zonca, A. Modelli, E. Varesi, T. Lowrey, A. Lacaita, G. Casagrande, P. Cappelletti, and R. Bez, in *Digest of Technical Papers. 2004 Symposium on VLSI Technology, 2004* (IEEE, 2004), pp. 18–19.

[12] M. Longo, R. Fallica, C. Wiemer, O. Salicio, M. Fanciulli, E. Rotunno, and L. Lazzarini, Nano Lett. **12**, 1509 (2012).

[13] B. Yu, X. Sun, S. Ju, D. B. Janes, and M. Meyyappan, IEEE Trans. Nanotechnol. **7**, 496 (2008).

[14] F. Xiong, M.-H. Bae, Y. Dai, A. Liao, A. Behnam, E. Carrion, S. Hong, D. Ielmini, and E. Pop, Nano Lett. **13**, 464 (2013).

[15]R. E. Simpson, P. Fons, A. V. Kolobov, T. Fukaya, M. Krbal, T. Yagi, and J. Tominaga, Nat. Nanotechnol. **6**, 501 (2011).

[16]A. L. Lacaita and D. J. Wouters, Phys. Status Solidi A **205**, 2281 (2008).

[17]H. P. Wong, S. Raoux, S. Kim, J. Liang, J. P. Reifenberg, B. Rajendran, M. Asheghi, and K. E. Goodson, Proc. IEEE **98**, 2201 (2010).

[18]S. Raoux, W. Wełnic, and D. Ielmini, Chem. Rev. **110**, 240 (2010).

[19]J. Reifenberg, E. Pop, A. Gibby, S. Wong, and K. Goodson, in *Thermal and Thermomechanical Proceedings 10th Intersociety Conference on Phenomena in Electronics Systems, 2006. ITHERM 2006* (IEEE, 2006), pp. 106–113.

[20]A. Faraclas, G. Bakan, L. Adnane, F. Dirisaglik, N. E. Williams, A. Gokirmak, and H. Silva, IEEE Trans. Electron Devices **61**, 372 (2014).

[21]D. L. Kencke, I. V. Karpov, B. G. Johnson, S. J. Lee, D. Kau, S. J. Hudgens, J. P. Reifenberg, S. D. Savransky, J. Zhang, M. D. Giles, and G. Spadini, in *2007 IEEE International Electron Devices Meeting* (IEEE, 2007), pp. 323–326.

[22]J. P. Reifenberg, D. L. Kencke, and K. E. Goodson, IEEE Electron Device Lett. **29**, 1112 (2008).

[23]J. P. Reifenberg, K. Chang, M. A. Panzer, S. Kim, J. A. Rowlette, M. Asheghi, H. P. Wong, and K. E. Goodson, IEEE Electron Device Lett. **31**, 56 (2010).

[24]D. G. Cahill, H. E. Fischer, T. Klitsner, E. T. Swartz, and R. O. Pohl, J. Vac. Sci. Technol. A **7**, 1259 (1989).

[25]D. G. Cahill, Rev. Sci. Instrum. **61**, 802 (1990).

[26]J. H. Kim, A. Feldman, and D. Novotny, J. Appl. Phys. **86**, 3959 (1999).

[27]L. Shi and A. Majumdar, ASME J. Heat Transfer **124**, 329 (2002).

[28]B. Cretin, S. Gomes, N. Trannoy, and P. Vairac, *Scanning Thermal Microscopy, Microscale and Nanoscale Heat Transfer Topics* (Springer-verlag, Berlin, 2007).

[29]H. M. Pollock and A. Hammiche, J. Phys. D: Appl. Phys. **34**, R23 (2001).

[30]H. Fischer, Thermochim. Acta **425**, 69 (2005).

[31]M. Nonnenmacher and H. K. Wickramasinghe, Appl. Phys. Lett. **61**, 168 (1992).

[32]S. Lefèvre and S. Voltz, Rev. Sci. Instrum. **76**, 033701 (2005).

[33]A. Majumdar, Annu. Rev. Mater. Sci. **29**, 505 (1999).

[34]A. Majumdar, J. P. Carrejo, and J. Lai, Appl. Phys. Lett. **62**, 2501 (1993).

[35]R. Aster, B. Borchers, and C. Thurber, *Parameter Estimation and Inverse Problems* (Elsevier Science, 2018).

[36]S. Deemyad and I. F. Silvera, Rev. Sci. Instrum. **79**, 086105 (2008).

[37]J.-L. Battaglia, A. Kusiak, V. Schick, A. Cappella, C. Wiemer, M. Longo, and E. Varesi, J. Appl. Phys. **107**, 044314 (2010).

[38]J.-L. Battaglia, V. Schick, C. Rossignol, A. Kusiak, I. Aubert, A. Lamperti, and C. Wiemer, Appl. Phys. Lett. **102**, 181907 (2013).

[39]J. J. Moré, in *Numerical Analysis*, edited by G. A. Watson (Springer, Berlin, 1978), pp. 105–116.

[40]R. H. Byrd, J. C. Gilbert, and J. Nocedal, Math. Program. **89**, 149 (2000).

[41]W. K. Hastings, Biometrika **57**, 97 (1970).

[42]R. D. Cowan, J. Appl. Phys. **32**, 1363 (1961).

[43]P.-E. Nordal and S. O. Kanstad, Phys. Scr. **20**, 659 (1979).

[44]J. Ishii, Y. Shimizu, K. Shinzato, and T. Baba, Int. J. Thermophys. **26**, 1861 (2005).

[45]J.-L. Battaglia, A. Kusiak, M. Bamford, and J.-C. Batsale, Int. J. Therm. Sci. **45**, 1035 (2006).

[46]N. Horny, M. Chirtoc, A. Fleming, G. Hamaoui, and H. Ban, Appl. Phys. Lett. **109**, 033103 (2016).

[47]H. G. Walther and T. Kitzing, J. Appl. Phys. **84**, 1163 (1998).

[48]A. Mandelis, J. Batista, and D. Shaughnessy, Phys. Rev. B **67**, 205208 (2003).

[49]S. Paoloni and D. Fournier, Rev. Sci. Instrum. **74**, 523 (2003).

[50]S. André, B. Rémy, D. Maillet, A. Degiovanni, and J.-J. Serra, J. Appl. Phys. **96**, 2566 (2004).

[51]M. Depriester, P. Hus, S. Delenclos, and A. H. Sahraoui, Rev. Sci. Instrum. **76**, 074902 (2005).

[52]R. Fuente, E. Apiñaniz, A. Mendioroz, and A. Salazar, J. Appl. Phys. **110**, 033515 (2011).

[53]K. Ghosh, A. Kusiak, P. Noé, M.-C. Cyrille, and J.-L. Battaglia, Phys. Rev. B **101**, 214305 (2020).

[54]A. Kusiak, J.-L. Battaglia, P. Noé, V. Sousa, and F. Fillot, J. Phys.: Conf. Ser. **745**, 032104 (2016).

[55]J.-L. Battaglia, A. Kusiak, C. Gaborieau, Y. Anguy, H. T. Nguyen, C. Wiemer, R. Fallica, D. Campi, M. Bernasconi, and M. Longo, Phys. Status Solidi RRL **10**, 544 (2016).

[56]J.-L. Battaglia, A. Kusiak, A. Saci, R. Fallica, A. Lamperti, and C. Wiemer, Appl. Phys. Lett. **105**, 121903 (2014).

[57]W. S. Capinski and H. J. Maris, Rev. Sci. Instrum. **67**, 2720 (1996).

[58]M. G. Burzo, P. L. Komarov, and P. E. Raad, J. Heat Transfer **124**, 1009 (2002).

[59]T. Baba, K. Ishikawa, T. Yagi, and N. Taketoshi, arXiv e-prints, arXiv:0709.1845 (2007).

[60]A. J. Schmidt, X. Chen, and G. Chen, Rev. Sci. Instrum. **79**, 114902 (2008).

[61]S. Dilhaire, G. Pernot, G. Calbris, J. M. Rampnoux, and S. Grauby, J. Appl. Phys. **110**, 114314 (2011).

[62]H.-K. Lyeo, D. G. Cahill, B.-S. Lee, J. R. Abelson, M.-H. Kwon, K.-B. Kim, S. G. Bishop, and B.-K. Cheong, Appl. Phys. Lett. **89**, 151904 (2006).

[63]M. Kuwahara, O. Suzuki, Y. Yamakawa, N. Taketoshi, T. Yagi, P. Fons, T. Fukaya, J. Tominaga, and T. Baba, Microelectron. Eng. **84**, 1792 (2007).

[64]J. P. Reifenberg, M. A. Panzer, S. Kim, A. M. Gibby, Y. Zhang, S. Wong, H.-S. P. Wong, E. Pop, and K. E. Goodson, Appl. Phys. Lett. **91**, 111904 (2007).

[65]Q. Li, J. Wei, H. Sun, K. Zhang, Z. Huang, and L. Zhang, Sci. Rep. **7**, 13747 (2017).

[66]R. J. Warzoha, B. F. Donovan, N. T. Vu, J. G. Champlain, S. Mack, and L. B. Ruppalt, Appl. Phys. Lett. **115**, 023104 (2019).

[67]E. Bozorg-Grayeli, J. P. Reifenberg, K. W. Chang, M. Panzer, and K. E. Goodson, in *2010 12th IEEE Intersociety Conference on Thermal and Thermomechanical Phenomena in Electronic Systems* (IEEE, 2010), pp. 1–7.

[68]C. Kim, D.-S. Suh, K. H. P. Kim, Y.-S. Kang, T.-Y. Lee, Y. Khang, and D. G. Cahill, Appl. Phys. Lett. **92**, 013109 (2008).

[69]W. J. Parker, R. J. Jenkins, C. P. Butler, and G. L. Abbott, J. Appl. Phys. **32**, 1679 (1961).

[70]J. A. Cape and G. W. Lehman, J. Appl. Phys. **34**, 1909 (1963).

[71]R. D. Cowan, J. Appl. Phys. **34**, 926 (1963).

[72]J. T. Schriempf, Rev. Sci. Instrum. **43**, 781 (1972).

[73]T. Azumi and Y. Takahashi, Rev. Sci. Instrum. **52**, 1411 (1981).

[74]Y. Takahashi, "Measurement of thermophysical properties of metals and ceramics by the laser-flash method," Int. J. Thermophys. **5**, 41–52 (1984).

[75]A. Degiovanni, G. Sinicki, and M. Laurent, "Heat pulse thermal diffusivity measurements-thermal properties temperature dependence and non-uniformity of the pulse heating," in *Thermal Conductivity 18*, edited by T. Ashworth and D. R. Smith (Springer US, Boston, MA, 1985), pp. 537–551.

[76]J. J. Hoefler and R. E. Taylor, Int. J. Thermophys. **11**, 1099 (1990).

[77]T. Baba, M. Kobayashi, A. Ono, J. Hong, and M. Suliyanti, Thermochim. Acta **218**, 329 (1993).

[78]T. Baba and A. Ono, Meas. Sci. Technol. **12**, 2046 (2001).

[79]L. Vozar, G. Labudova, and W. Hohenauer, Int. J. Thermophys. **23**, 1157 (2002).

[80]D. Maillet, S. André, J.-C. Batsale, A. Degiovanni, and C. Moyne, *Thermal Quadrupoles: Solving the Heat Equation Through Integral Transforms* (Wiley, 2000).

[81]J.-L. Battaglia, E. Ruffio, A. Kusiak, C. Pradere, E. Abisset, S. Chevalier, A. Sommier, and J.-C. Batsale, Measurement **158**, 107691 (2020).